International Journal of Environmental Science and Technology (2022) 19:9901–9914
https://doi.org/10.1007/s13762-021-03816-y

ORIGINAL PAPER

Yttrium oxide-doped ZnO for effective adsorption of basic fuchsin dye: equilibrium, kinetics, and mechanism studies

M. A. Ben Aissa[1] · L. Khezami[2,3] · K. Taha[4] · N. Elamin[2,5] · B. Mustafa[1,6] · A. S. Al-Ayed[1] · A. Modwi[1]

Received: 19 November 2020 / Revised: 6 October 2021 / Accepted: 15 November 2021 / Published online: 27 November 2021

Abstract

The ability of yttrium oxide-doped zinc oxide nanoparticles (YZnO) to eliminate Basic Fuchsin dye (BF) from wastewater was investigated. YZnO was obtained by a mechanical ball milling approach. The X-ray diffraction pattern revealed a wurtzite ZnO structure with the appearance of the Y2O3 phase and a crystallite size reduction from 20 to 16 nm. The morphology of the fabricated nanoparticles exhibited increasingly agglomerated particles. The specific surface area increases with doping from 10.13 to 20.62 $m^2\ g^{-1}$, leading to enhance the adsorption capacity of the Yttrium-doped ZnO as opposed to pure ones. The initial BF concentration and pH influenced the removal efficiency resulting in 75.53 mg/g of YZnO adsorption capacity at pH = 11 and 180 min of equilibrium time. These results register that YZnO is an effective sorbent for the elimination of BF from wastewater. The pseudo-second-order model ideally suited the kinetic data, and the adsorption equilibrium was established to conform with the Freundlich isotherm. The BF adsorption mechanism is associated with the electrostatic interaction and hydrogen bond, as indicated by the pH, the coexisting ions, and the FTIR studies.

Keywords Basic Fuchsin removal · Electrostatic interactions · Elimination mechanism · Y_2O_3-doped ZnO

Introduction

The need for potable water is immensely expanding with the increasing human population. The inevitable textile, pigment and paint release substantial amounts of hazardous dyes to the aquatic system (Tan et al. 2015). Dyes represent a large portion of these pollutants, as about 15% of the 70 million tons of annual production of dyes run into watercourses (Yuan et al. 2020a, b). Consequently, the discharge of these unsafe wastes into the environment jeopardizes human health, causing respiratory problems, skin irritation, and cancer risk (de Lima Barizão et al. 2020; Lou et al. 2020). Moreover, dyes prompt a great chemical oxidation demand causing a nasty odor in wastewater (Midha and Dey 2008). The basic fuchsin (BF), also known as Rosaniline chloride or Basic Violet (Lee and Ong 2017), belongs to the triarylmethane class and possesses a great planar conjugated π-system (Soneta et al. 2006). It is a cationic dye used in various fields such as coloring agents in textile industries, biological stains, paper. (Hunger 2007; Ong et al. 2012). Nonetheless, the basic fuchsin (BF) dye possesses inflammable, anesthetic, and bacterial characteristics (Pathrose et al. 2016; Yamil et al. 2020). Also, due to its weak biodegradation, carcinogenicity, and toxicity (Huang et al. 2012), it has been considered a suspected carcinogen in many countries (Yang et al. 2015). Hence, great attention has been drawn to the elimination of BF from wastewater.

Conventional strategies such as filtration membrane (Aziz et al. 2020), electrochemical processing (Gökkuş 2016; de

Editorial responsibility: Senthil Kumar Ponnusamy.

✉ M. A. Ben Aissa
dalibenissa@gmail.com

1 Department of Chemistry, College of Science and Arts at Al-Rass, Qassim University, Buraydah, Saudi Arabia

2 Department of Chemistry, College of Sciences, Imam Mohammad Ibn Saud Islamic University (IMSIU), Riyadh 11623, Saudi Arabia

3 LaNSER, Research and Technology Centre of Energy (CRTEn), Borj Cedria Technopark, BP. 95, 2050 Hammam-Lif, Tunisia

4 College of Applied & Industrial Sciences, Chemical & Industrial Chemistry Department, Bahri University, Khartoum, Sudan

5 Chemistry Department, Sudan University of Science and Technology College of Science, Khartoum, Sudan

6 Department of Chemistry, Faculty of Science and Technology, Alneelain University, Khartoum, Sudan

Almeida et al. 2019), coagulation-flocculation (Gökkuş and Yıldız 2014; Iloamaeke et al. 2021), and aerobic (Castro et al. 2020) are adopted to get rid of these dye contaminants. However, these standard procedures have quite a lot of disadvantages, such as ineffectiveness and a high cost. Instead. Adsorption is an inexpensive and remarkably effective method for eliminating pollutants (Çelebi 2019; Yuan et al. 2020a, b). Natural adsorbents, agricultural wastes, and palm oil waste are utilized for contaminant adsorption and removal (Ai et al. 2011; Ali 2018; Mehr et al. 2020). The efficacy of the adsorption method on the dye's elimination count upon serval factors such as the dyes concentration, pH, coexisting ions, stirring speed, sorbent dose, contact time, and temperature. For example, Bessashia et al. investigated the influence of the eggshell membrane dose, BF initial concentration, temperature, pH, stirring speed, and contact time on the BF elimination from water (Bessashia et al. 2020). Recently, nanomaterials are employed to discard these hazardous materials from water and wastewater systems (Ashouri et al. 2019). Researchers are seriously charmed with the ZnO for its outstanding characteristics, including the raised binding energy (60 m eV) and sweeping band gap (≈ 3.4 eV) (Sangeetha et al. 2015). ZnO nanoparticles have exhibited an important adsorption affinity toward divers dyes (Chaudhary et al. 2016; Zhang et al. 2016; Palai et al. 2021). Several searches have been carried to explore doped nanomaterials as efficient sorbents for removing dyes from used water. However, doping modifies the proprieties of doped material compared to pure ones, such as the porosity and the surface area, driving to improve adsorption capacity (AC) (Klett et al. 2014; Guan et al. 2019). For instance, it has used several dopants such as chitosan ZnO NPs to remove Direct Blue 78, and Acid Black 26 (Salehi et al. 2010), Mg-doped ZnO (Rath et al. 2019) for the elimination of Congo red, and Pb-doped ZnO as a good adsorbent for Reactive Black 5 (Dassi et al. 2020). However, the utilization of yttrium-doped ZnO NPs, as a potential sorbent for the BF elimination from wastewater, has not yet been published. Therefore, this project aims for the first time to use synthesized Y_2O_3-doped ZnO (YZnO) for the elimination of BF from aqueous media and investigate the adsorption mechanism of BF.

In this work, YZnO nanoparticles were obtained using a mechanical ball milling approach and were characterized by different techniques (SEM, XRD, BET, and FTIR). The synthesized YZnO was used to eliminate BF dye from aqueous media. For this aim, the influences of the efficient parameters such as pH, initial BF concentration, and coexisting ions will be optimized. The adsorption kinetics will be modeled using four equations: pseudo-first-order, pseudo-second-order, intra-particle diffusion and Elovich. Meanwhile, Temkin, Dubinin–Radushkevich, Elovich, Freundlich, and Langmuir models were utilized to assess the experimental equilibrium. The mechanism of BF sorption on YZnO will also be examined.

Materials and methods

Preparation of YZnO and ZnO

ZnO NPs were obtained via the sol–gel method. First, zinc acetate (39.9 mmoles) was dissolved in a methanol–water mixture (3:1) and agitated for 15 min. Hereafter, a saturated starch solution (30 mL) was appended dropwise, and the blending was stirred until the sol was made. Afterward, 60 ml of the aqueous tartaric acid (66 mmoles) was supplemented dropwise up to gel formation. The collected gel was dried at 105 °C for 10 h. Afterward, the obtained powder was crushed and annealed for 3 h at 500 °C.

YZnO NPs were prepared through a solid-state reaction with stoichiometric amounts of Y_2O_3 and ZnO by milling in a high-energy planetary mill. The milling process was realized in Fritsch Pulverisette P5 at room temperature for 24 h. The ball-to-powder weight ratio was appointed to 20:1, and the rotational speed was maintained at 450 rpm.

Adsorption experiments details

Experimental Kinetic and equilibrium studies were detailed in the supplementary information. The kinetic study is carried out using the different models, such as pseudo-first-order, pseudo-second-order, intra-particle diffusion, and Elovich. Detailed equations of the used models are listed in Table S1. Temkin, Dubinin–Radushkevich, Elovich, Freundlich, and Langmuir models were employed to assess the experimental equilibrium, and its detailed equations are given in Table S2.

Results and discussion

Structural description of nanomaterials

XRD characterization

The XRD patterns of YZnO and ZnO NPs divulge sharp diffraction peaks, indicating the obtaining of highly crystalline nanostructures. The peaks emerging at $2\theta \approx 69$, 68, 66, 62, 56, 47, 36, 34 and 31° can be, respectively, designated to the (201), (112), (200), (102), (103), (110), (101), (002), and (100) characteristics planes of wurtzite hexagonal ZnO (Swarthmore 1972). Besides, the impurity peaks (indicated as * in Fig. 1 corresponding to the Y_2O_3 phase) developed due to doping process, connoting that Y was not fully incorporated into the host ZnO lattice, showing phase segregation

(Kumar et al. 2015). The appearance of the phase peak (≈ 29 °) indicates the formation of this separate phase. Moreover, the two XRD patterns comparing show diffraction peaks shift owing to the doping to lower values. Whenever the positive charge is higher, the repulsion increases, leading to diffraction angle reduction and inter-planar spacing widening. (Ye et al. 2013). A similar shift of (002) peaks was assigned to the modification of lattice parameters (Yang et al. 2008). The crystallite sizes obtained from Scherrer's equation were 24.88 and 19.89 nm for YZnO and ZnO, respectively (Barrett 1943). The larger crystallite size of YZnO NPs than the undoped ZnO (Table 1) is consistent with the substitution of the smaller size Zn^{2+} (0.074 nm) with a larger ionic radius Y^{3+} (0.090 nm) through the doping process (Zheng et al. 2012). The lattice parameters a $a(=\lambda/\sqrt{3}.sin\theta_{(100)})$ and $c(=\lambda/sin\theta_{(002)})$ (Modwi et al. 2018) are larger for ZnO. The lattice imperfection and/or distortions $\varepsilon = \beta/4cos\theta$ increased with Y doping lead to an increase in crystallite size (Mote et al. 2012). The microstrain (ε_z) follows the same tendency of the microstrain (Karthika and Ravichandran 2015).

SEM, EDX and X-ray elemental mapping of YZnO and ZnO

The SEM images of YZnO and pure ZnO (Fig. 2a, b) exhibit an irregular spherical shape with little crystallized dimension nanoparticles. On the other hand, the agglomeration increased for the YZnO with the growth of non-uniform particle configuration. EDX analysis (Fig. 2c, d) was applied to detect the elements existing in ZnO and YZnO nanomaterials. The spectra portrayed sharp signals at 0.5 and 1 keV related to (O) and (Zn) for ZnO (Modwi et al. 2019), and 2, 1, and 0.5 keV for Y, Zn, and O, respectively. Besides, the small peak at 8.5 keV was due to the Zn surface plasmon resonance.

The element's weight proportions attained from the EDX results are presented in Table 2, and the findings were affirmed to be in suitable accordance with the composition.

The X-ray elemental results of YZnO (Y, Zn, and O) were determined by EDX area scanning (Fig. 3a–c). The spectra were visibly confirmed by homogeneously distributed Y_2O_3 on the ZnO nanoparticles. Additionally, the X-ray elemental mapping of Zn, O, and Y was well defined with sharp contrast, indicating the successful mixing of Y_2O_3 with ZnO surface and the formation of YZnO composite construction.

Surface area analysis of YZnO and ZnO

The surface and porosity properties of prepared nanomaterials were recorded employed BET along with that BJH graph. The isotherms correspond to Langmuir type II (Fig. 4a–b) with relative pressure (P/Po = 0.025–0.1), as displayed from obtained N2 sorption isotherms. Besides, the hysteresis loop is type H3 (Fig. 4a–b inset pore distribution) that confirms the mesoporous characteristic of material with slit-shape pores (Lippens and De Boer 1965). All graphs are positioned in the range of 25–160 nm, which is in accordance with the type II adsorption isotherm following IUPAC classification (Sotomayor et al. 2018). The effect of Y_2O_3 loaded into the ZnO nanomaterials has increased the specific surface area from 10.12 to 20.62 $m^2\ g^{-1}$. Additionally, the pore distribution and the pore volume of the two samples equal to 23.46 and 29.75 nm, as well as 0.066 and 0.1641 cm^3g^{-1}, respectively. It can be shown that the YZnO structure has an evident influence on the pore size distribution and the surface area, leading to enhanced AC of the yttrium-doped ZnO as opposed to pure ones.

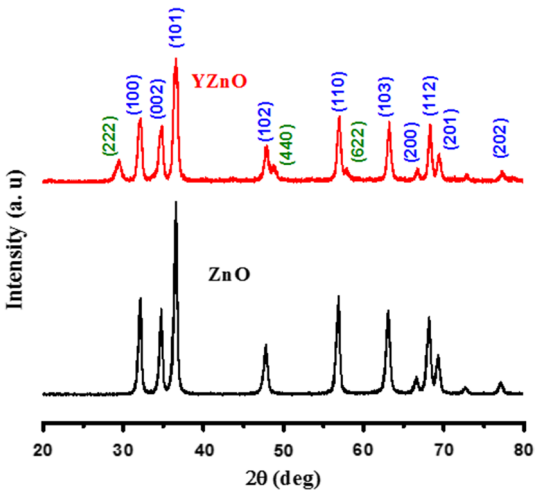

Fig. 1 XRD patterns for YZnO and ZnO

Table 1 The 2θ (101), β, IY, D, c, a and v values of the nanoparticles

Samples	2θ (101)	Intensity	FWHM	D (nm)	Lattice parameters		*c/a*	Unit cell (*v*)
					a	*c*		
ZnO	36.550	740	0.447	19.54	3.257	5.222	1.6033	47.972
YZnO	36.534	323	0.528	15.85	3.209	5.152	1.6055	45.944

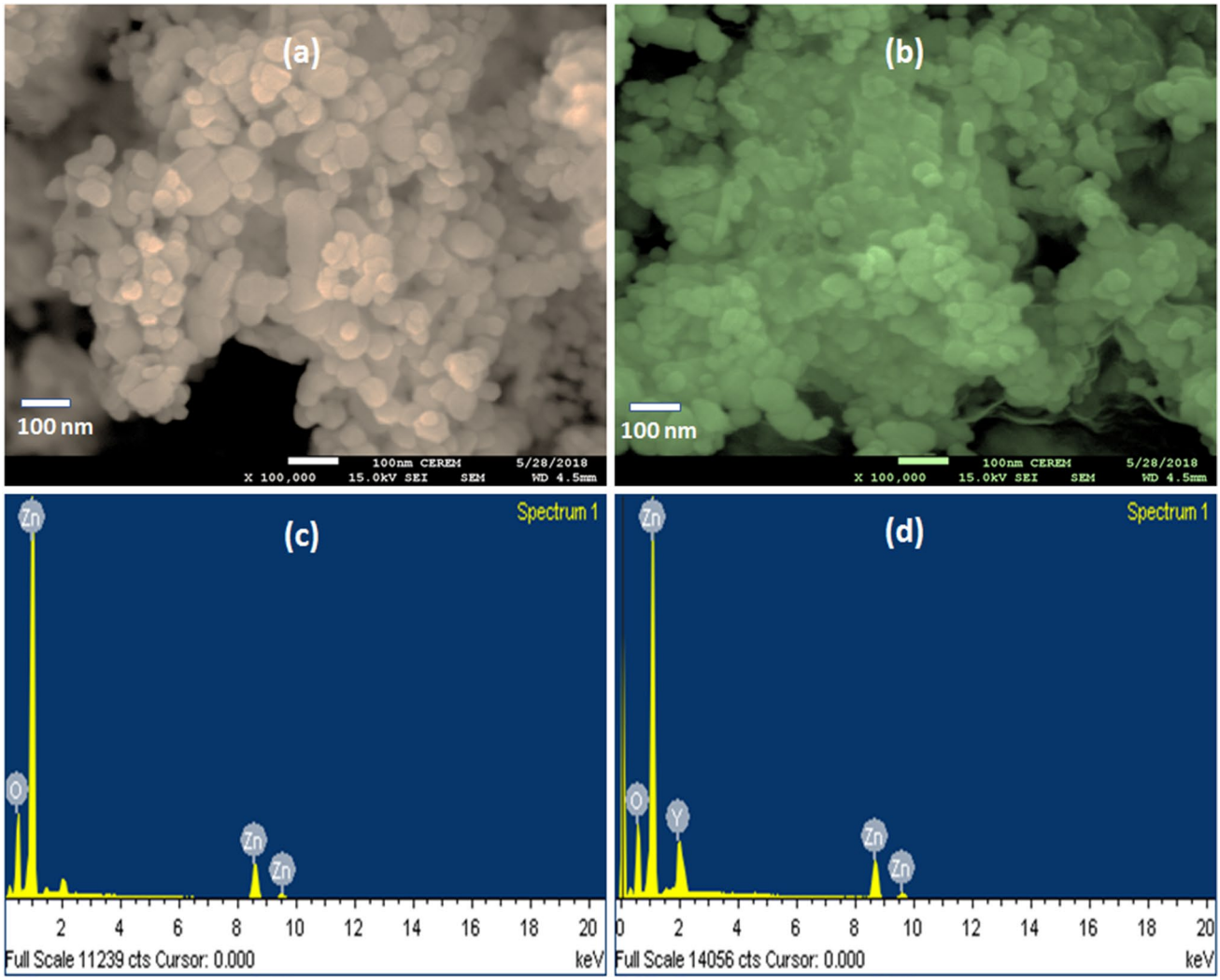

Fig. 2 SEM images and EDX of ZnO (**a**), (**c**) and YZnO nanopowders (**b**), (**d**)

Table 2 Percentage elements weight

Nanomaterials	Percentage weight (%)		
	O	Zn	*Y*
ZnO	21.70	78.30	0
YZnO	20.33	66.06	13.61

Adsorption of BF

Influence of BF concentration

Experiments are preceded at a temperature of 25 °C and pH = 7 with different concentrations and a constant amount of adsorbent (15 mg of YZnO in 25 mL of dye solution). The BF concentration varied from 5 to 100 ppm. The obtained results (Fig. 5a) show that the adsorbed quantity of BF increases from 7.83 to 75.70 mg g^{-1} if the dye concentration increased. Herein, the effective driving force produced by increasing the initial BF concentration surmounts any resistance to BF molecules migration from the solution. The resulting fractional adsorption becomes reliant to the initial concentration (Elkady et al. 2011; Bessashia et al. 2020).

Influence of pH on BF adsorption

The pH's influence on BF adsorption onto YZnO is given in Fig. 5b. As shown, the upmost adsorption efficiency was obtained at higher pH values, and when the pH value decreased, the uptake decreased rapidly. The optimal pH for the BF elimination from an aqueous solution was 11. The pH_{ZPC} value of YZnO was ≈ 6.3 (pH_{ZPC} presents the

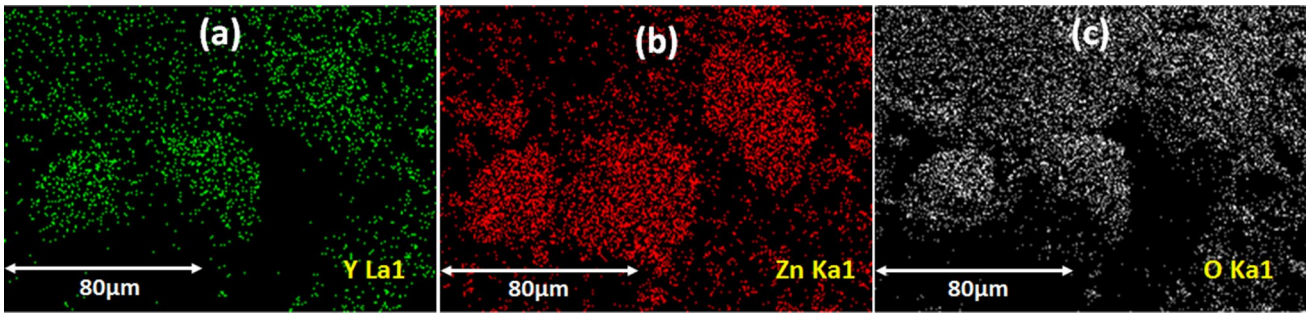

Fig. 3 X-ray elemental mapping of (**a**) Y–La, (**b**) Zn–Ka, and (**c**) O–Ka

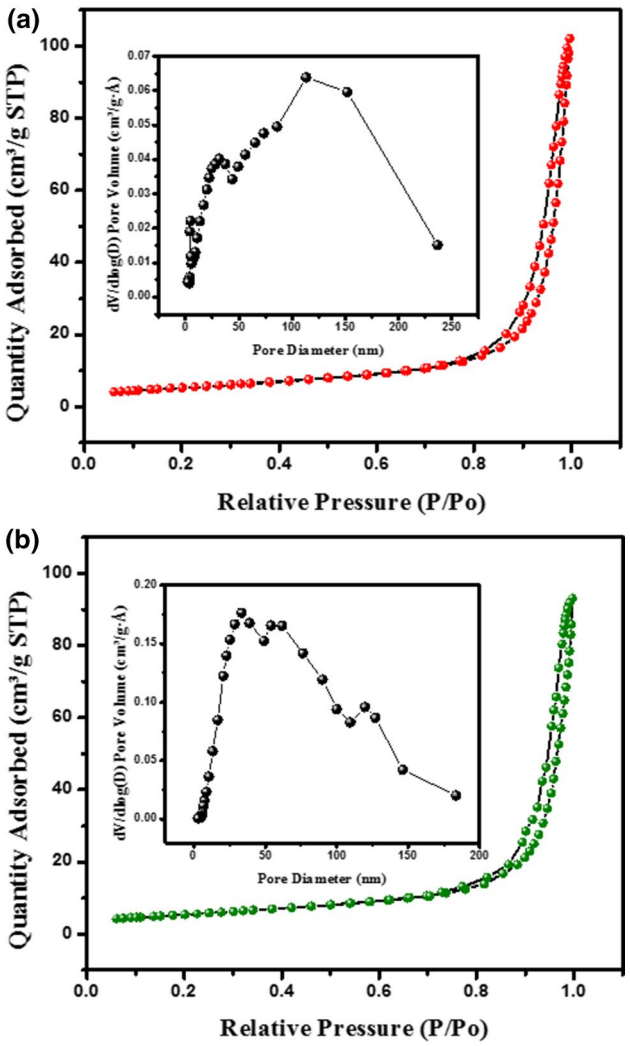

Fig. 4 N_2 adsorption–desorption cures (inset BJH plots showing pore distribution) of ZnO (**a**) and YZnO (**b**)

pH when the surface charge on the YZnO is zero (Fig. 5c)). Accordingly, there develops an electrostatic repulsion between the sorbent and the BF dye at lower pH values leading to low adsorption efficiency (Futamata et al. 2011). The electrostatic attraction between YZnO and BF dye enhances the dye's adsorption at higher pH (Moawed and Alqarni 2013). Therefore, the positive charge on the cationic dye makes them prone to the attraction by the negatively charged surface at pH above the pH_{ZPC} (Tahir and Rauf 2006). Analogous trends on the elimination of cationic dyes were previously reported for MB (Hameed and Ahmad 2009; Mittal et al. 2014) and methyl orange (Shen et al. 2015).

Influence of coexisting ions

Wastewater always included, along with dye, a broad category of coexisting ions that can influence the adsorption process of dyes. Therefore, to investigate the impact of coexisting cations on BF adsorption onto YZnO, NaCl and $MgCO_3$ were chosen as commonly coexisting salts, and the experiments were carried out using two concentrations of cations (25 and 50 ppm). From Fig. 5d, it was established that the addition of Na^+ and Mg^{2+} cations leads to a decrease in the BF elimination efficiency. Moreover, the elimination efficiency of BF decreased when concentration changed from 25 to 50 ppm from 89 to 80% with Na^+ and from 70 to 50% with Mg^{2+}. The results moreover affirmed the electrostatic interaction of BF with YZnO, in accordance with the result obtained in the pH study.

Kinetic study

The contact time impact on the adsorption process onto YZnO was explored at BF concentration of 25 ppm and for shaking time from 0 to 1440 min. Figure 5e exhibits a continuous decrease in the population of BF monomers (λmax = 545 nm) and the BF dimers (λmax = 486 nm) as the

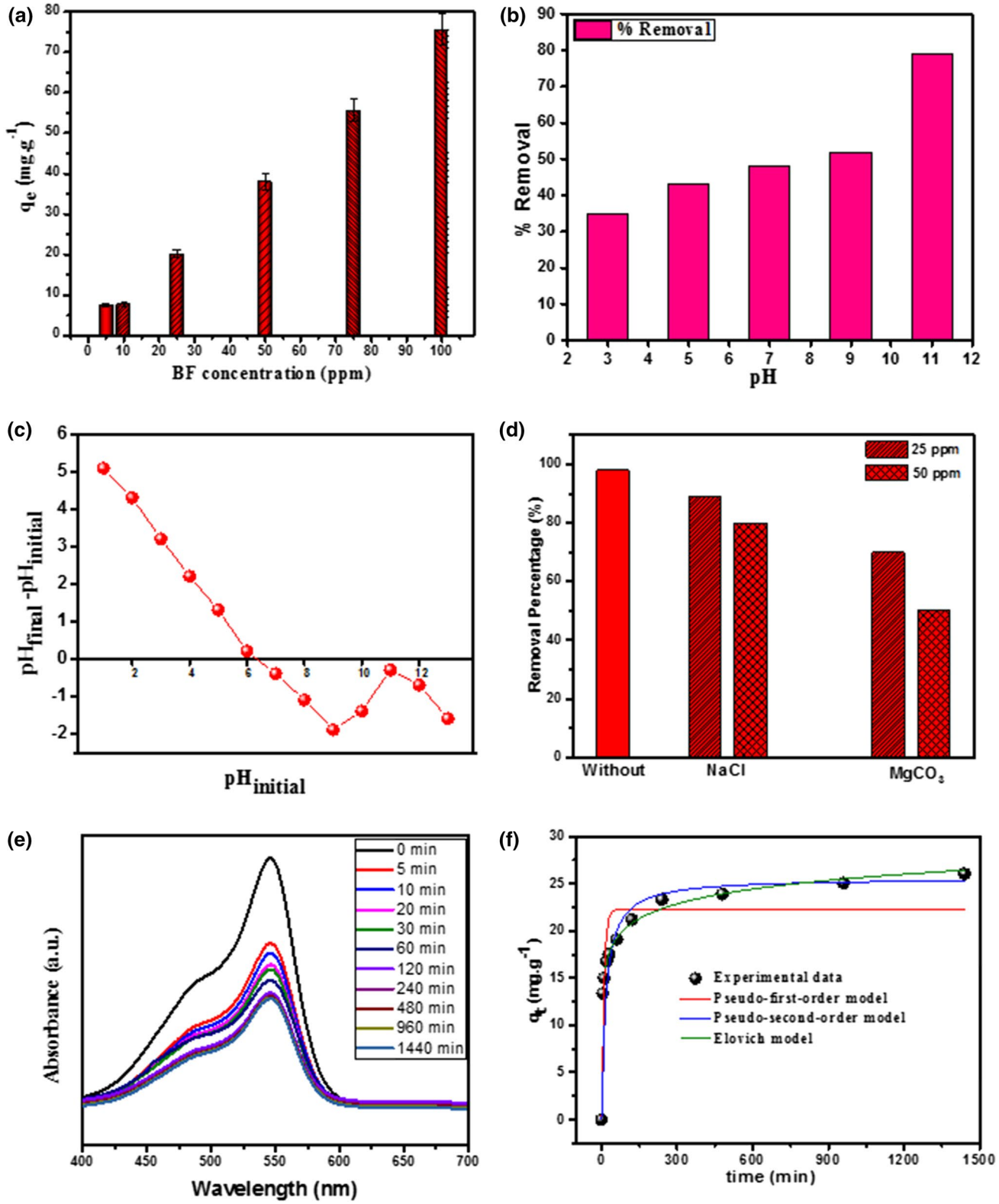

Fig. 5 Influence of initial **b** BF dye concentration on the adsorption on YZnO (**a**), influence of pH on % elimination of BF (**b**), plot for the determination of pHZPC of YZnO (**c**), influence of coexisting cations on BF elimination efficiency by YZnO (pH = 11 and BF concentration = 25 ppm) (**d**),UV–Vis kinetic spectrum adsorption of BF on YZnO (**e**) and equilibrium time models comparison (**f**)

Table 3 Used kinetics models for BF adsorption by YZnO

Kinetics model	Parameters	Values	R^2
Pseudo 1st order	q_e	9.22 mg g^{-1}	0.8851
	K_1	1.7×10^{-3} min^{-1}	
Pseudo 2nd order	q_e	26.02 mg g^{-1}	0.9991
	K_2	2.01×10^{-3} g mg^{-1} min^{-1}	
	h_0	5.23×10^{-2} mg g^{-1} min^{-1}	
	$t_{1/2}$	19.12 min	
Elovich	β	0.4414 g mg^{-1}	0.9904
	α	182.35 mg g^{-1} min^{-1}	
Intra-particle Diffusion	K_{dif1}	0.851 mg g^{-1} $min^{1/2}$	0.9578
	C_1	12.34	
	K_{dif2}	0.123 mg g^{-1} $min^{1/2}$	0.9942
	C_2	21.32	

adsorption progressed (Singha et al. 2017). As given from Fig. 5f, the AC increases quickly within the initial 150 min and achieves equilibrium at about 180 min.

The low correlation coefficient ($R^2 = 0.8851$ (Table 3)) and the deviation of the AC from the experimental data conclude the inapplicability of pseudo-first-order kinetics to the adsorption of BF onto YZnO. The great value of R^2 (= 0.9991) and the nearness of the calculated q_e (= 26.02 mg g^{-1}) compared to the experimental q_e value (25.20 mg g^{-1}) indicate the agreement of the pseudo-second-order kinetic with adsorption (Zamouche et al. 2020). The shorter half-sorption time ($t_{1/2} = 1/(k_2.q_e) = 19.20$ min) and the high initial rate of sorption ($h_0 = k_2.q_e^2 = 0.0523$ mg g^{-1} min^{-1}) are evidence of favored high rate adsorption of the dye (Li et al. 2012).

Testing experimental data for fitting with the *Elovich* equation is done by plotting q_t versus $ln\ t$. The great value of R^2 (= 0.9904) for the linear plot indicates the correspondence of the experimental data with the *Elovich* model (Ho and McKay 2004). The R^2 values are more than 0.96, signifying the pertinence of the data to the model. However, the linear plot does not pass per the origin, suggesting another sorption modes involvement (Okello et al. 2017).

The intra-particle diffusion graph (Fig. 6) is multi-linear reflected by the two sorption stages (Yazdani et al. 2016). The sharp first stage may have developed from the dye transport from the BF solution to the external YZnO surface via limit layer, whereas the secondary stage can designate the ultimate equilibrium as the intra-particle diffusion begins to decrease owing to the reduced BF concentration gradient. Table 3 exhibits a lessening in diffusion rate at a long contact time owing to the small pores available for diffusion as the BF molecules formerly pass into the inside voids of YZnO, that proved through the lesser k_{dif2} value as opposed to k_{dif1}. The higher C value in secondary stage conjectures a bigger limit layer influence. (Milosavljević et al. 2011). Thus, the surface and limit layer sorption or intra-particle diffusion contribute to dye elimination by adsorbent (Ali et al. 2018a, b).

Adsorption equilibrium

Adsorption isotherm parameters are presented in Table 4. The highest regression coefficient ($R^2 = 0.9957$) and the good fitting of the line (Fig. 7) designate the accordance of the data with *Freundlich* isotherm (Vijayaraghavan et al. 2006).

The large magnitude of the exponent $n > 2$ provides a clue on the favorability of adsorption as commonly asserted that n values in the gamut 2–10 signify excellent adsorption characteristics (Treybal 1980). The higher R^2 (= 0.9957) for the Freundlich model than Langmuir model ($R^2 = 0.9611$) advocates adsorption on the YZnO heterogeneous surface rather than monolayer adsorption (Ali et al. 2018a, b). The adsorption process is attributed, whether it is primarily physical or chemical, according to the value of E in the Dubinin–Radushkevich isothermal model (Demiral et al. 2008). The physical adsorption happens when the E value is fewer than eight kJ mol^{-1} (Mondal and Basu 2019), while the process is chemisorption when the E value is among 8 and 16 kJ mol^{-1} (Zhang et al. 2019). The calculated mean energy value (E) was 7.23 kJ mol^{-1}, confirming that the process of BF adsorption on YZnO was defined as physical.

For the utilization in the field, it is beneficial to compare the AC of YZnO with various sorbents available for BF. Table 5 displays the AC of several sorbents for BF elimination confronted with the YZnO. It is noticeable that the AC of the YZnO is higher than reported sorbents, such as industrial sludges and Fe-MgO-coated kaolinite. This result

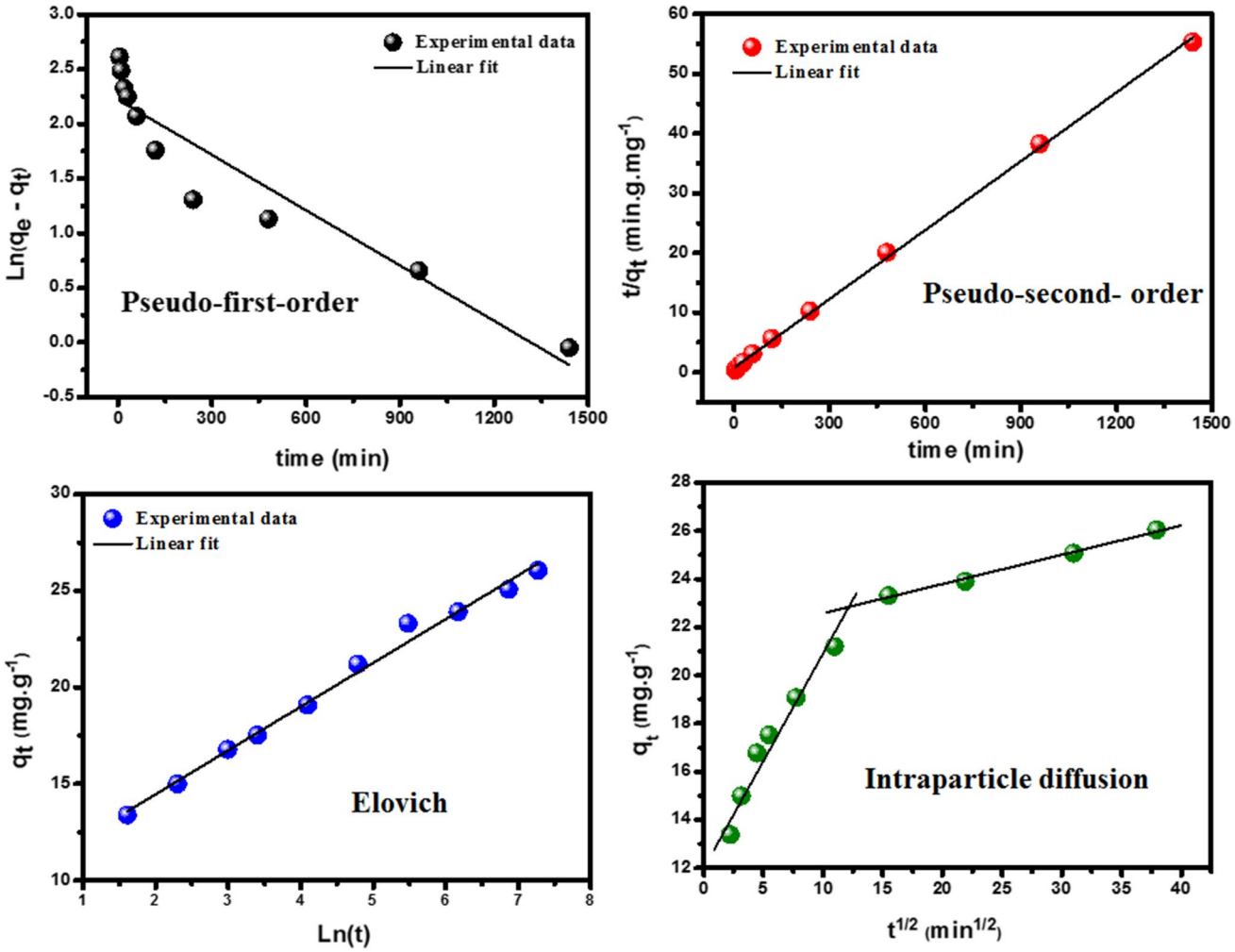

Fig. 6 Kinetics data of BF adsorption onto YZnO

Table 4 Used isotherm model for BF adsorption onto YZnO

Equilibrium model	Parameters	Values	R^2
Langmuir	q_m	75.53 mg g^{-1}	0.961
	K_L	0.0927 mg g^{-1}	
	R_L	0.125 L mg^{-1}	
Freundlich	K_F	9.96 L mg^{-1}	0.996
	n	2.12	
Temkin	B	190.1 J mol^{-1}	0.914
	K_T	1.81 L mg^{-1}	
Elovich	q_m	26.73 mg g^{-1}	0.892
	K_E	0.455 L mg^{-1}	
Dubinin- Radushkevich	q_m	71.0 mg g^{-1}	0.953
	β	9.56×10^{-9} (mol $KJ^{-1})^2$	
	E	7.23 kJ mol^{-1}	

revealed that YZnO is an effective adsorbent for BF, giving a high potential for dye removal in wastewater.

Adsorption mechanism The study of the pH's influence implies that the electrostatic attraction could dominate (control) the mechanism adsorption of BF onto YZnO. The BF molecules and YZnO surface were identically charged at low pH values, impeding BF adsorption owing to the electrostatic repulsions. The adsorption efficiency noted at pH < pHZPC proves the existence of other interactions between BF and YZnO. Furthermore, the two primary amine in the molecular structure of BF can establish hydrogen bonds with OH groups of YZnO (Al-Ghouti et al. 2003). Therefore, two reverse mechanisms (hydrogen bonding and electrostatic repulsions) can occur simultaneously at the YZnO surface. However, it can be shown that the BF removal was

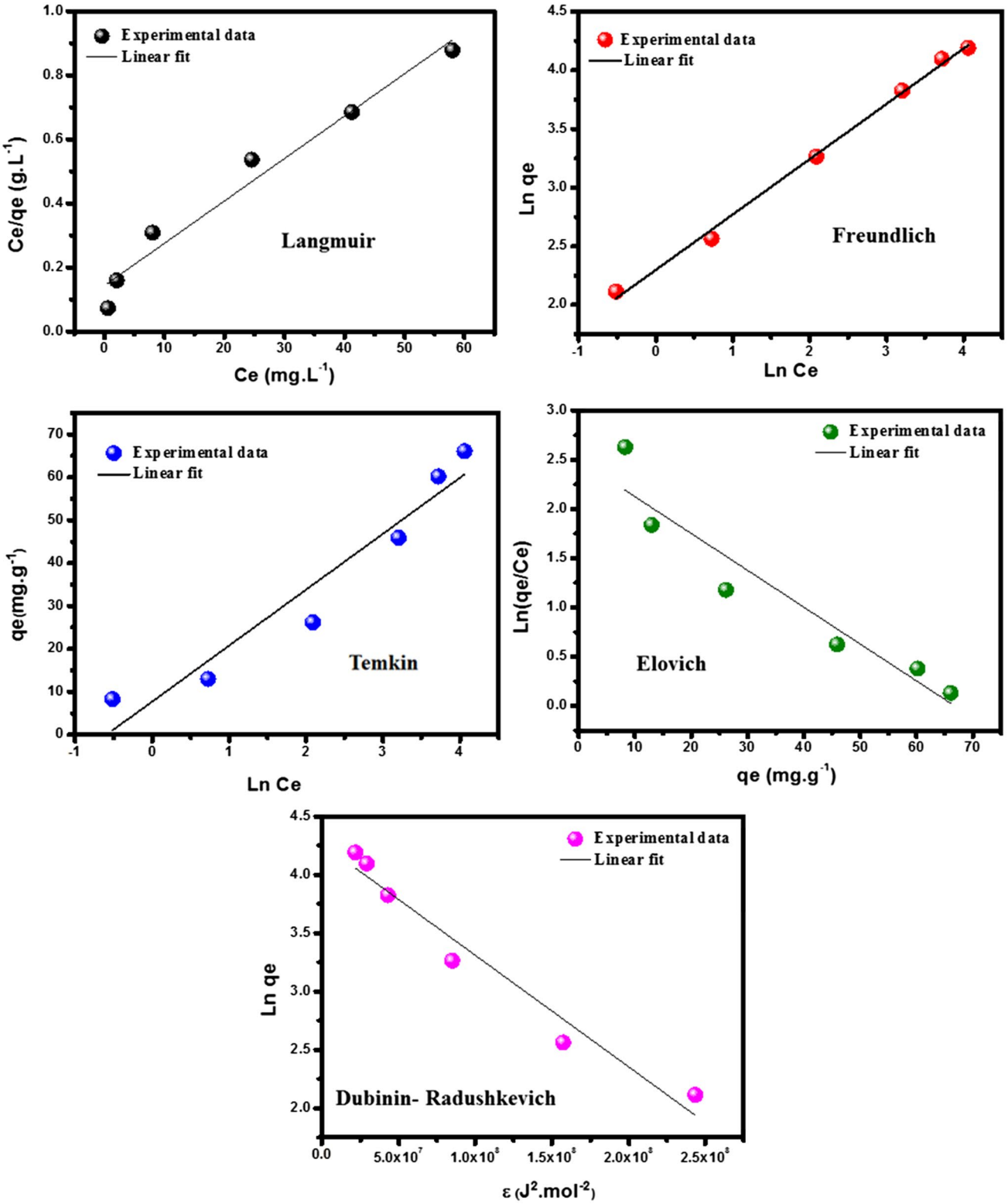

Fig. 7 Adsorption of BF equilibrium models

Table 5 BF adsorption capacities of several sorbents

Sorbents	AC (mg/g)	Reference
Industrial sludges	70.40	Seredych and Bandosz (2007)
Super absorbent polymer	11.70	Dhodapkar et al. (2007)
Deoiled soya	12.00	Gupta et al. (2008)
Bottom ash	6.40	Gupta et al. (2008)
Sodium sulfite modified cationexchange resin	127.00	Bayramoglu et al. (2009)
Graphite oxide	1.83	Qin et al. (2014)
Fe-MgO/kaolinite	10.36	Khan and Khan (2015)
Starch-capped zinc selenide nanoparticles	222.70	Sharifpour et al. (2020)
Al/MCM-41	54.44	Guan et al. (2018)
Fe/ZSM-5	251.87	Mohammed et al. (2020)
SBA-16	39.61	Guan et al. (2019)
Al/SBA-16	70.08	Guan et al. (2019)
ESM	47.85	Bessashia et al. (2020)
YZnO nanoparticles	75.53	This study

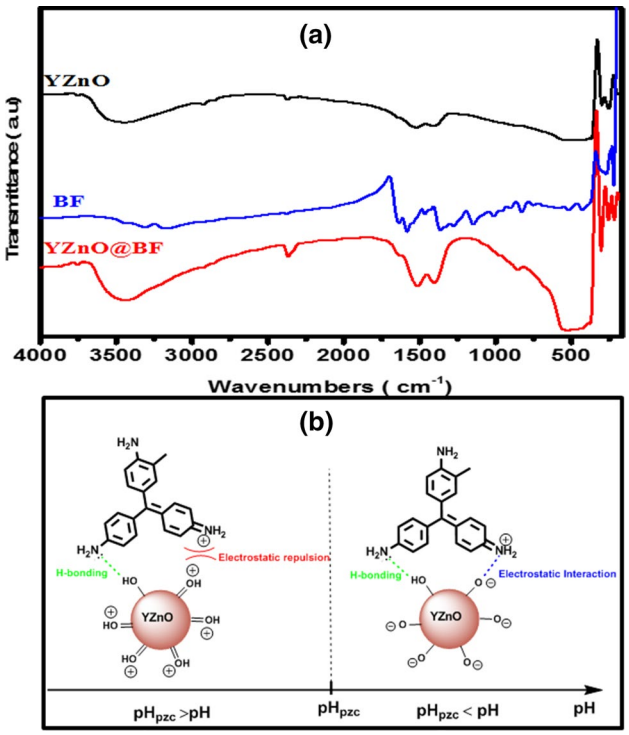

Fig. 8 FTIR spectra of YZnO, BF, and YZnO @BF (**a**) and proposed adsorption mechanism of BF onto YZnO NPs (**b**)

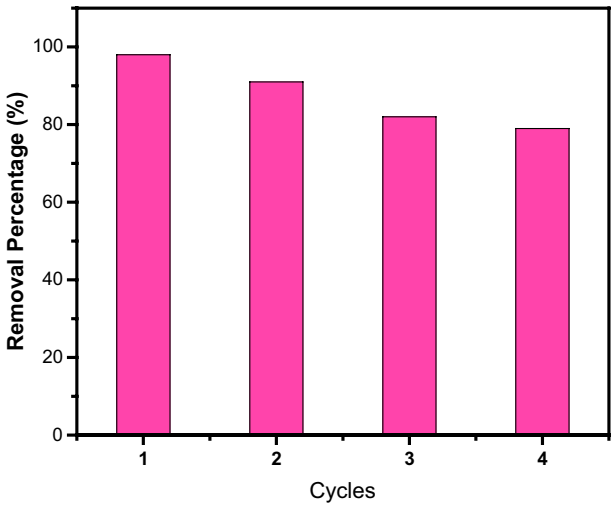

Fig. 9 Reusability Efficiency of YZnO NPs

increased at a pH higher than 6.3; this can be due to hydrogen bonds and the electrostatic attractions between YZnO and BF molecules. FTIR spectra of YZnO, BF, and YZnO@BF (Fig. 8a) were registered in the range of 200–4000 cm^{-1} to additionally explain the adsorption mechanism. BF spectrum (Fig. 8a) shows many bands that can be distinguished as follow: aryl CH wagging (904–837 cm^{-1}), C=N stretching (1630; 1328 cm^{-1}), and NH_2 bending (3296; 1567 cm^{-1}) (Mohammed and Yahia 2018). The YZnO spectrum (displayed in Fig. 8a) presents an important band at 3485 cm^{-1} attributed to the O–H stretching vibration of water in ZnO (Khezami et al. 2017). After BF adsorption, the stretching

O–H band slightly shifted to 3456 cm^{-1} owing to the presence of hydrogen bond interactions between the lone-pair electrons of amine groups of BF and OH groups of YZnO (Singha et al. 2017). In addition, several characteristic bands of the BF have appeared and changed positions compared to those of the free molecules indicating that interactions may exist between BF and YZnO. For example, the apparition of a novel band at 1641 cm^{-1} in YZnO@BF spectra implied the establishment of ionic interactions between the negative YZnO charged surface and amino groups of BF dyes (Singha et al. 2017). Liu et al. have proved that the cationic dyes are adsorbed via electrostatic attraction (Liu et al. 2020). The recommended sorption mechanism of the BF onto the YZnO involves hydrogen bonds and the electrostatic attractions between OH groups on the YZnO surface and BF molecules. (Fig. 8b).

Regeneration/reusability experiments

Since cyclic availability is an important property, it is necessary to testify the regeneration and the reusability of an adsorbent. The used YZnO composite was regenerated by calcination for one hour at 500 °C. After the adsorption experiment, the used YZnO was recuperated by filtration and then calcinated at 500 °C before it was reused. Figure 9 shows the reusability results. It is found that YZnO has effectively employed for the BF elimination, at least in four continual cycles.

Conclusion

In this work, the YZnO nanoparticle, as an effective sorbent for the BF elimination, was obtained using a mechanical ball milling and was characterized. The sorption experiments were achieved to examine the influence of initial BF concentration, the coexisting ions, and pH. The effect of initial BF concentration had an important effect on BF sorption onto YZnO, and the % BF elimination was established to increase remarkably with pH. The equilibrium time of YZnO was 180 min, and the adsorption amount of YZnO was 75.53 mg g^{-1} at the optimum pH equal to 12. The great values of R^2 indicate the compliance of adsorption to the pseudo-second-order kinetic and Freundlich isotherm models. The adsorption mechanism of BF is associated with the electrostatic interaction and hydrogen bond, as indicated by the pH, the coexisting ions, and the FTIR studies. BF adsorption capacities of YZnO compared to those detailed in the literature predicted that YZnO is an effective adsorbent for BF and has great potential application in BF dye elimination. Hence, YZnO could be an effective sorbent to eliminate other cationic dyes such as Crystal violet, Auramine O, and Malachite green.

Supplementary Information The online version contains supplementary material available at https://doi.org/10.1007/s13762-021-03816-y.

Acknowledgements The current study was carried thanks to the support of the department of Chemistry, College of Science and Arts, Al-Rass, Qassim University.

Declarations

Conflict of interest We declare that we do not have any commercial or associative interest that could potentially affect the submitted work.

References

Ai L, Zhang C, Liao F, Wang Y, Li M, Meng L, Jiang J (2011) Removal of methylene blue from aqueous solution with magnetite loaded multi-wall carbon nanotube: Kinetic, isotherm and mechanism analysis. J Hazard Mater 198:282–290

Al-Ghouti M, Khraisheh M, Allen S, Ahmad M (2003) The removal of dyes from textile wastewater: A study of the physical characteristics and adsorption mechanisms of diatomaceous earth. J Environ Manage 69(3):229–238

Ali S (2018) Fabrication of a nanocomposite from an agricultural waste and its application as a biosorbent for organic pollutants. IJEST 15(6):1169–1178

Ali I, Peng C, Ye T, Naz I (2018a) Sorption of cationic malachite green dye on phytogenic magnetic nanoparticles functionalized by 3-marcaptopropanic acid. RSC Adv 8(16):8878–8897

Ali MEA, Aboelfadl MMS, Selim AM, Khalil HF, Elkady GM (2018b) Chitosan nanoparticles extracted from shrimp shells, application for removal of fe (ii) and mn (ii) from aqueous phases. Separ Sci Tech 53(18):2870–2881

Ashouri R, Ghasemipoor P, Rasekh B, Yazdian F, Mofradnia SR (2019) The effect of zno-based carbonaceous materials for degradation of benzoic pollutants: A review. IJEST 16(3):1729–1740

Aziz, H., H. Tajarudin, T. Wei and M. Alazaiza, 2020. Iron and manganese removal from groundwater using limestone filter with iron-oxidized bacteria. IJEST: 1–14.

Barrett CS (1943) Structure of metals. McGraw-Hill Book Company, Inc., New York

Bayramoglu G, Altintas B, Arica MY (2009) Adsorption kinetics and thermodynamic parameters of cationic dyes from aqueous solutions by using a new strong cation-exchange resin. Chem Eng J 152(2–3):339–346

Bessashia, W., Y. Berredjem, Z. Hattab and M. Bououdina, 2020. Removal of basic fuchsin from water by using mussel powdered eggshell membrane as novel bioadsorbent: Equilibrium, kinetics, and thermodynamic studies. Environ. Res.: 109484.

Castro, F., J. Bassin, T. Alves, G. Sant'Anna and M. Dezotti, 2020. Reactive orange 16 dye degradation in anaerobic and aerobic mbbr coupled with ozonation: Addressing pathways and performance. IJEST: 1–20.

Çelebi H (2019) The applicability of evaluable wastes for the adsorption of reactive black 5. IJEST 16(1):135–146

Chaudhary S, Kaur Y, Umar A, Chaudhary GR (2016) Ionic liquid and surfactant functionalized zno nanoadsorbent for recyclable proficient adsorption of toxic dyes from waste water. J Mol Liq 224:1294–1304

Dassi, R.B., B. Chamam, J. Méricq, C. Faur, L. El Mir, I. Trabelsi and M. Heran, 2020. Novel polyvinylidene fluoride/lead-doped zinc oxide adsorptive membranes for enhancement of the removal of reactive textile dye. IJEST: 1–12.

de Almeida E, de Andrade A, Corso C (2019) Evaluation of the acid blue 161 dye degradation through electrochemical oxidation combined with microbiological systems. IJEST 16(12):8185–8196

de Lima Barizão, A.C., M.F. Silva, M. Andrade, F.C. Brito, R.G. Gomes and R. Bergamasco, 2020. Green synthesis of iron oxide nanoparticles for tartrazine and bordeaux red dye removal. J. Environ. Chem. Eng., 8(1): 103618.

Demiral H, Demiral I, Tümsek F, Karabacakoğlu B (2008) Adsorption of chromium (vi) from aqueous solution by activated carbon derived from olive bagasse and applicability of different adsorption models. Chem Eng J 144(2):188–196

Dhodapkar R, Rao N, Pande S, Nandy T, Devotta S (2007) Adsorption of cationic dyes on jalshakti®, super absorbent polymer and photocatalytic regeneration of the adsorbent. React Funct Polym 67(6):540–548

Elkady M, Ibrahim AM, Abd El-Latif M (2011) Assessment of the adsorption kinetics, equilibrium and thermodynamic for the potential removal of reactive red dye using eggshell biocomposite beads. Desalination 278(1–3):412–423

Futamata M, Yu Y, Yajima T (2011) Elucidation of electrostatic interaction between cationic dyes and ag nanoparticles generating enormous sers enhancement in aqueous solution. J Phys Chem C 115(13):5271–5279

Gökkuş Ö (2016) Oxidative degradation of basic black 3 by electrogenerated fenton's reagent using carbon fiber cathode. Clean Technol Environ Policy 18(5):1525–1534

Gökkuş Ö, Yıldız Y (2014) Investigation of the effect of process parameters on the coagulation-flocculation treatment of textile wastewater using the taguchi experimental method. Fresenius Environ Bull 23(2):463–470

Guan Y, Wang S, Wang X, Sun C, Wang Y, Hu L (2018) Preparation of mesoporous al-mcm-41 from natural palygorskite and its adsorption performance for hazardous aniline dye-basic fuchsin. Micropor Mesopor Mat 265:266–274

Guan Y, Wang S, Sun C, Yi G, Wu X, Chen L, Ma X (2019) Wet chemical extraction of silicon from natural palygorskite for preparing a mesoporous molecular sieve of al-sba-16. CHEM PAP 73(11):2655–2666

Gupta V, Mittal A, Gajbe V, Mittal J (2008) Adsorption of basic fuchsin using waste materials—bottom ash and deoiled soya—as adsorbents. J Colloid Interface Sci 319(1):30–39

Hameed B, Ahmad A (2009) Batch adsorption of methylene blue from aqueous solution by garlic peel, an agricultural waste biomass. J Hazard Mater 164(2–3):870–875

Ho Y, McKay G (2004) Sorption of copper (ii) from aqueous solution by peat. Water Air Soil Pollut 158(1):77–97

Huang L, Kong J, Wang W, Zhang C, Niu S, Gao B (2012) Study on fe (iii) and mn (ii) modified activated carbons derived from zizania latifolia to removal basic fuchsin. Desalination 286:268–276

Hunger K (2007) Industrial dyes: Chemistry, properties, applications. John Wiley & Sons

Iloamaeke, I.M., N.J. Nnaji, E.C. Okpala, A.N. Eboatu and T.U. Onuegbu, 2021. Mercenaria mercenaria shell: Coagulation-flocculation studies on colour removal by response surface methodology and nephlometric kinetics of an industrial effluent. J. Environ. Chem. Eng.: 105715.

Karthika K, Ravichandran K (2015) Tuning the microstructural and magnetic properties of zno nanopowders through the simultaneous doping of mn and ni for biomedical applications. J Mater Sci Technol 31(11):1111–1117

Khan TA, Khan EA (2015) Removal of basic dyes from aqueous solution by adsorption onto binary iron-manganese oxide coated kaolinite: Non-linear isotherm and kinetics modeling. Appl Clay Sci 107:70–77

Khezami L, Taha KK, Modwi A (2017) Efficient removal of cobalt from aqueous solution by zinc oxide nanoparticles: Kinetic and thermodynamic studies. Z Naturforsch A 72(5):409–418

Klett C, Barry A, Balti I, Lelli P, Schoenstein F, Jouini N (2014) Nickel doped zinc oxide as a potential sorbent for decolorization of specific dyes, methylorange and tartrazine by adsorption process. J Environ Chem Eng 2(2):914–926

Kumar P, Singh V, Sharma V, Rana G, Malik HK, Asokan K (2015) Investigation of phase segregation in yttrium doped zinc oxide. Ceram in 41(5):6734–6739

Lee, H.-J. and S.-T. Ong, 2017. Immobilization of rambutan (nephelium lappaceum) peel as a sorbent for basic fuchsin removal. Environ. Prot. Eng., 43(1).

Li N, Mei Z, Wei X (2012) Study on sorption of chlorophenols from aqueous solutions by an insoluble copolymer containing β-cyclodextrin and polyamidoamine units. Chem Eng J 192:138–145

Lippens BC, De Boer J (1965) Studies on pore systems in catalysts: V. The t Method J Catal 4(3):319–323

Liu Y, Zhao Y, Cheng W, Zhang T (2020) Targeted reclaiming cationic dyes from dyeing wastewater with a dithiocarbamate-functionalized material through selective adsorption and efficient desorption. J Colloid Interface Sci 579:766–777

Lou, L., R.J. Kendall and S. Ramkumar, 2020. Comparison of hydrophilic pva/tio2 and hydrophobic pvdf/tio2 microfiber webs on the dye pollutant photo-catalyzation. J. Environ. Chem. Eng.: 103914.

Mehr H, Saffari J, Mohammadi S, Shojaei S (2020) The removal of methyl violet 2b dye using palm kernel activated carbon: Thermodynamic and kinetics model. IJEST 17(3):1773–1782

Midha V, Dey A (2008) Biological treatment of tannery wastewater for sulfide removal. Int J Chem Sci 6(2):472–486

Milosavljević NB, Ristić MĐ, Perić-Grujić AA, Filipović JM, Štrbac SB, Rakočević ZL, Krušić MTK (2011) Removal of cu 2+ ions using hydrogels of chitosan, itaconic and methacrylic acid: Ftir, sem/edx, afm, kinetic and equilibrium study. Colloids Surf, A Physicochem Eng Asp 388(1):59–69

Mittal H, Ballav N, Mishra SB (2014) Gum ghatti and fe3o4 magnetic nanoparticles based nanocomposites for the effective adsorption of methylene blue from aqueous solution. J Ind Eng Chem Res 20(4):2184–2192

Moawed EA, Alqarni Y (2013) Determination of azine and triphenyl methane dye in wastewater using polyurethane foam functionalized with tannic acid. Sample Prep 1(2013):18–27

Modwi, A., M. Ali, K.K. Taha, M. Ibrahem, H. El-Khair, M. Eisa, M. Elamin, O. Aldaghri, R. Alhathlool and K. Ibnaouf, 2018. Structural and optical characteristic of chalcone doped zno nanoparticles. J. Mater. Sci.: Mater. Electron., 29(4): 2791–2796.

Modwi, A., K.K. Taha, L. Khezami, A.S. Al-Ayed, O. Al-Duaij, M. Khairy and M. Bououdina, 2019. Structural and electrical

characterization of ba/zno nanoparticles fabricated by co-precipitation. JIOPM: 1–12.
Mohammed, B.B., A. Hsini, Y. Abdellaoui, H. Abou Oualid, M. Laabd, M. El Ouardi, A.A. Addi, K. Yamni and N. Tijani, 2020. Fe-zsm-5 zeolite for efficient removal of basic fuchsin dye from aqueous solutions: Synthesis, characterization and adsorption process optimization using bbd-rsm modeling. J. Environ. Chem. Eng., 8(5): 104419.
Mohammed M, Yahia I (2018) Synthesis and optical properties of basic fuchsin dye-doped pmma polymeric films for laser applications: Wide scale absorption band. Opt Quantum Electron 50(3):159
Mondal NK, Basu S (2019) Potentiality of waste human hair towards removal of chromium (vi) from solution: Kinetic and equilibrium studies. Appl Water Sci 9(3):1–8
Mote V, Purushotham Y, Dole B (2012) Williamson-hall analysis in estimation of lattice strain in nanometer-sized zno particles. J Theor Appl Phys 6(1):6
Okello, V.A., S.J. Kimosop, Z.M. Getenga, F. Orata and V.O. Shikuku, 2017. Green remediation of carbamazepine from water using novel magnetic iron modified carbonized baggasse: Kinetics, equilibrium and mechanistic studies.
Ong S-T, Tan S-Y, Khoo E-C, Lee S-L, Ha S-T (2012) Equilibrium studies for basic blue 3 adsorption onto durian peel (durio zibethinus murray). Desalination Water Treat 45(1–3):161–169
Palai P, Muduli S, Priyadarshini B, Sahoo TR (2021) A facile green synthesis of zno nanoparticles and its adsorptive removal of congo red dye from aqueous solution. Mater Today: Proc 38:2445–2451
Pathrose B, Nampoori V, Radhakrishnan P, Mujeeb A (2016) Investigations on the third order nonlinear optical properties of basic fuchsin dye using zscan technique. Optik 127(19):7717–7725
Qin J, Qiu F, Rong X, Yan J, Zhao H, Yang D (2014) Removal of basic fuchsin dye from aqueous solutions using graphite oxide modified aromatic polyurethane foam material. TOXICOL ENVIRON CHEM 96(6):849–860
Rath P, Behera S, Priyadarshini B, Panda S, Mandal D, Sahoo T, Mishra S, Sahoo TR, Parhi P (2019) Influence of mg doping on zno nps for enhanced adsorption activity of congo red dye. Appl Surf Sci 491:256–266
Salehi R, Arami M, Mahmoodi NM, Bahrami H, Khorramfar S (2010) Novel biocompatible composite (chitosan–zinc oxide nanoparticle): Preparation, characterization and dye adsorption properties. Colloids Surf b: Biointerfaces 80(1):86–93
Sangeetha, R., S. Muthukumaran and M. Ashokkumar, 2015. Structural, optical, dielectric and antibacterial studies of mn doped zn 0.96 cu 0.04 o nanoparticles. SAA: Molecular and Biomolecular Spectroscopy, 144: 1–7.
Seredych M, Bandosz TJ (2007) Removal of cationic and ionic dyes on industrial− municipal sludge based composite adsorbents. Ind Eng Chem Res 46(6):1786–1793
Sharifpour E, Ghaedi M, Asfaram A, Farsadrooh M, Dil EA, Javadian H (2020) Modeling and optimization of ultrasound-assisted high performance adsorption of basic fuchsin by starch-capped zinc selenide nanoparticles/ac as a novel composite using response surface methodology. Int J Biol Macromol 152:913–921
Shen J, Li Z, Wu Y-N, Zhang B, Li F (2015) Dendrimer-based preparation of mesoporous alumina nanofibers by electrospinning and their application in dye adsorption. Chem Eng J 264:48–55
Singha NR, Karmakar M, Mahapatra M, Mondal H, Dutta A, Roy C, Chattopadhyay PK (2017) Systematic synthesis of pectin-g-(sodium acrylate-co-n-isopropylacrylamide) interpenetrating polymer network for superadsorption of dyes/m (ii): Determination of physicochemical changes in loaded hydrogels. Polym Chem 8(20):3211–3237
Soneta Y, Midorikawa T, Miyamura K (2006) Anomalous distortion and stacking column formation of [ni (dmit) 2]− induced by propeller-shaped dye cations, crystal violet and basic fuchsin. Bull Chem Soc Jpn 79(7):1060–1062
Sotomayor FJ, Cychosz KA, Thommes M (2018) Characterization of micro/mesoporous materials by physisorption: Concepts and case studies. Acc Mater Surf Res 3(2):36–37
Swarthmore, P., 1972. Powder diffraction file, joint committee on powder diffraction standards. International center for diffraction data. Card: 3–0226.
Tahir S, Rauf N (2006) Removal of a cationic dye from aqueous solutions by adsorption onto bentonite clay. Chemosphere 63(11):1842–1848
Tan KB, Vakili M, Horri BA, Poh PE, Abdullah AZ, Salamatinia B (2015) Adsorption of dyes by nanomaterials: Recent developments and adsorption mechanisms. SEP PURIF TECHNOL 150:229–242
Treybal, R.E., 1980. Mass transfer operations. New York, 466.
Vijayaraghavan K, Padmesh T, Palanivelu K, Velan M (2006) Biosorption of nickel (ii) ions onto sargassum wightii: Application of two-parameter and three-parameter isotherm models. J Hazard Mater 133(1–3):304–308
Yamil, L.d.O., J. Georgin, G.S. Dos Reis, É.C. Lima, M.L. Oliveira, D.S. Franco, M.S. Netto, D. Allasia and G.L. Dotto, (2020) Utilization of pacara earpod tree (enterolobium contortisilquum) and ironwood (caesalpinia leiostachya) seeds as low-cost biosorbents for removal of basic fuchsin. Environ Sci Pollut Res 27(26):33307–33320
Yang J, Gao M, Yang L, Zhang Y, Lang J, Wang D, Wang Y, Liu H, Fan H (2008) Low-temperature growth and optical properties of ce-doped zno nanorods. APPL SURF SCI 255(5):2646–2650
Yang X, Li Y, Du Q, Sun J, Chen L, Hu S, Wang Z, Xia Y, Xia L (2015) Highly effective removal of basic fuchsin from aqueous solutions by anionic polyacrylamide/graphene oxide aerogels. J Colloid Interface Sci 453:107–114
Yazdani MR, Tuutijärvi T, Bhatnagar A, Vahala R (2016) Adsorptive removal of arsenic (v) from aqueous phase by feldspars: Kinetics, mechanism, and thermodynamic aspects of adsorption. J Mol Liq 214:149–156
Ye Z-Y, Lu H-L, Geng Y, Gu Y-Z, Xie Z-Y, Zhang Y, Sun Q-Q, Ding S-J, Zhang DW (2013) Structural, electrical, and optical properties of ti-doped zno films fabricated by atomic layer deposition. Nanoscale Res Lett 8(1):1–6
Yuan, H., L. Chen, Z. Cao and F.F. Hong, 2020. Enhanced decolourization efficiency of textile dye reactive blue 19 in a horizontal rotating reactor using strips of bnc-immobilized laccase: Optimization of conditions and comparison of decolourization efficiency. Biochem. Eng. J., 156: 107501.
Yuan, J., Y. Amano and M. Machida, 2020. Study on the characteristics of nitrogen-doped activated carbon fibers to remove nitrate ions by multi-factor analysis. IJEST: 1–8.

Zamouche M, Habib A, Saaidia K, Lehocine MB (2020) Batch mode for adsorption of crystal violet by cedar cone forest waste. SN Appl Sci 2(2):198

Zhang F, Chen X, Wu F, Ji Y (2016) High adsorption capability and selectivity of zno nanoparticles for dye removal. Colloids and Surfaces A. Physicochem Eng Asp 509:474–483

Zhang H, Hu J, Xie J, Wang S, Cao Y (2019) A solid-state chemical method for synthesizing mgo nanoparticles with superior adsorption properties. RSC Adv 9(4):2011–2017

Zheng J, Song J, Jiang Q, Lian J (2012) Enhanced uv emission of y-doped zno nanoparticles. Appl Surf Sci 258(18):6735–6738